

Examination for the MPhil Degree: Certificate of Dissertation Submission



UNIVERSITY OF
CAMBRIDGE

Board of Graduate Studies

You are required to complete Part I of this form, in capital letters, and upload it, with your MPhil Degree thesis, to the relevant authority responsible for receiving your dissertation.

Please ensure that you keep your contact information up to date on the Personal Portfolio part of your Self-Service pages as interested parties may need to communicate with you at short-notice regarding your oral examination, where to send results and documentation. You will also need to keep the office to which you submit this form informed of any change in contact details.

PART I For completion by student

Name **Oliver O'Reilly-Hyland**

College: **Lucy Cavendish**

Title of MPhil examination for which you are a candidate

Dissertation.....

Title of dissertation* **Fine Scale Fuel Design**

*This title should correspond exactly with that on the title page.

In order to comply with the Regulations for the Degree you are required to make the following declarations by signing below:

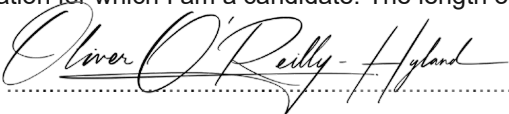
Other purpose (if any) to which the work has been put¹

I hereby declare that:

- this dissertation is the result of my own work and includes nothing which is the outcome of work done in collaboration except where specifically indicated in the text and bibliography
- my dissertation is not substantially the same as any that I have submitted, or, is being concurrently submitted for a degree or diploma or other qualification at the University of Cambridge or any other University or similar institution. I further state that no substantial part of my dissertation has already been submitted, or, is being concurrently submitted for any such degree, diploma or other qualification at the University of Cambridge or any other University of similar institution

Statement of word /length²

I hereby declare that my dissertation does not exceed the limit of length prescribed in the Special Regulations of the MPhil examination for which I am a candidate. The length of my dissertation is

Signed 

Date24/9/24.....

Address for Examination Purposes

Telephone number

Email address

Notes

1. If you are unable to subscribe to the second sentence of this declaration you should, in the preface of the dissertation, say which parts have already been, or are being concurrently submitted for a degree, diploma or other qualification at any other University.
2. You are reminded that there is no provision in the Regulations for exceeding the prescribed word limit.

PART II For completion by the authority responsible for receiving the dissertation

Those Degree Committee or departmental offices responsible for receiving dissertations should complete this section and return this form to the Board of Graduate Studies, 4 Mill Lane, Cambridge, CB2 1RZ as soon as possible.

I certify that the dissertation was submitted to the appropriate authority on:

Signed

Date

For use by the office of the Board of Graduate Studies only

Graduate Student No:

Record amended :

Multi-Objective Evolutionary Design of Enrichment Gradients and Burnable Absorber Distributions



Oliver O'Reilly-Hyland

Supervisor: Dr. Geoffrey Parks

Department of Engineering

This dissertation is submitted for the degree of
Master of Philosophy

Lucy Cavendish College

September 2024

Abstract

The advent of additive manufacturing (AM) techniques has enabled the fabrication of complex fuel geometries with unprecedented precision. This study explores the optimization of nuclear fuel design using AM to produce gradients of fissile material and burnable absorbers to improve fuel utilization and reduce reactivity swing. A multi-objective evolutionary algorithm is employed to optimize enrichment and burnable absorber distributions in a standard AP1000 fuel assembly, with the objective of maximizing end-of-life criticality (EoL K_{eff}) and minimizing reactivity swing and assembly power peaking factor (PPF). The presence of burnable absorbers was found to obscure the effect of enrichment distribution, and further study is needed to disentangle their effects. The optimization studies revealed a consistent trend of better performance with absorbers towards the center and more enrichment towards the center, highlighting the potential benefits of central-absorber alternatives to traditional outer-layer integrated fuel burnable absorber designs (IFBA). This study provides a comprehensive framework for optimizing nuclear fuel design using AM and burnable absorbers, and opens up new avenues for research in fuel performance improvement.

Table of contents

List of figures	vii
List of tables	viii
1 Introduction	1
1.1 Introduction	1
1.2 Advanced Nuclear Fuel Fabrication	3
1.2.1 Fine-Scale Burnable Absorber Gradients	6
1.2.2 Fine-Scale Additives, Dopants, and Porosity Gradients	7
1.3 Modeling	8
2 Research Objectives	9
3 Design Considerations	11
4 Methodology	13
4.1 Homogeneous Fuel Assembly Benchmarking	13
4.2 Integration of DEAP with OpenMC for Fuel Assembly Optimization	14
4.2.1 Optimization Case Studies Overview	14
4.2.2 Fuel Assembly Modeling	15
4.2.3 Script Parameters and Integration	16
4.2.4 Objective Functions and Constraints:	16
4.3 Computational Workflow	18
4.4 Adjustments and Optimization Strategies	18
5 Results	21
5.1 Study A: Fine-Scale Multi-Objective Optimization of Enrichment and Gadolinia Zoning	21
5.1.1 Results A Discussion	21

Table of contents	vi
5.2 CSBA Case Study	26
6 Conclusion	30
References	32
Appendix A	37

List of figures

4.1	The graphics above illustrate the zoned fuel assembly	20
5.1	Enrichment & Gadolinium Study Convergence Plot	21
5.2	Fuel Enrichment values Over Generations	23
5.3	3D Pareto Front for BOL Keff, EOL Keff. and PPF	23
5.4	Pareto Front for EOL KEFF vs PPF	24
5.5	U238 Absorption Rate Radial Profile	24
5.6	Burnup vs PPF ove 18months for Design II	24
5.7	Normalized Fission Rate Radial Distribution for Objective I	25
5.8	Enrichments for 2nd Optimization Funciton	26
5.9	Homogeneous 7.13% vs Optimized Fuel Assembly Design	26
5.10	Separated Optimization Convergence: Avg pop	27
5.11	Burnup vs PPF for best individual (18 months; 109 days per step, crude) . .	27
5.12	Optimized Inputs for CSBA	28
5.13	CSBA: A Flatter Radial Distribution of Fission	29
6.1	CSBA Opti is Study B, CSBA Homo is its Homogeneous equivalent, UB2 Peripheral is the same boron overall volume, swapped into outer zone 4. . .	30
A.1	PPF vs BoL Keff Pareto Front, Study A	37
A.2	Final generation pareto front Case Study A	37
A.3	3D pareto front for BoL Keff, EoL Keff, and PPF	37
A.4	UB2 No Bo Depletion Study	38
A.5	Hypervolume progression over generations	38
A.6	PPF vs EoL Keff pareto front	38
A.7	UB2 layer radius v. atom fraction in UB2 (failed study; UB2 not depletable in this one, hence 100 generations)	38

List of tables

1.1	AM Fuel architecture applications and characteristics	4
1.2	Benefits, challenges, and progress of additive manufacturing (AM).	5
4.1	Performance of Homogeneous AP1000 Fuel Assembly	13
4.2	Genetic Algorithm Parameters and Population Settings for Optimization Runs	17
4.3	Optimization Constraints and Variable Limits for Fuel zones and UO ₂ /UB ₂ layer	19
4.4	Axial Zones and Layer Options for Fuel and Burnable Absorber Distribution	19
5.1	Optimized Fuel	22
5.2	Optimized Reactor Performance Metrics	25
5.3	Optimized CSBA UB ₂ Design Metrics	28

Chapter 1

Introduction

1.1 Introduction

Until recently, optimizing a nuclear core has been constrained by economic and practical manufacturing considerations [1]. The design space for nuclear reactor cores has recently expanded thanks to more advanced computational codes and the easing of conventional manufacturing limitations, specifically more complex distributions of traditional and nontraditional materials [2]. This enhanced design space, facilitated by additive and future manufacturing methods, demands the use of optimization algorithms [3–6].

Thanks to progress in Additive Manufacturing (AM) methods, the distribution of fissile materials and burnable absorbers can be optimized in any dimension; not just within an assembly, but also within the fuel meat of individual fuel pellets [7]. This represents a possibility to shift from coarser assembly-level optimizations to a finer-scale optimization, where designers can directly target neutronic phenomena at the individual fuel pin and even intra-pin scale with more specific distributions and concentrations of fissile materials, burnable absorbers, and other features and additives [8]. Among localized effects at this finer scale, spatial self-shielding presents a significant opportunity for improvement through detailed fuel design optimization [3, 8].

Self-shielding in nuclear fuel, comprising resonance and spatial effects, significantly influences neutron absorption in fuel elements due to the nature of energy-dependent cross-sections of nuclear materials. Resonance self-shielding occurs when neutron absorption cross-sections exhibit sharp peaks at specific energies, causing local neutron flux depressions. Spatial self-shielding refers to neutron flux attenuation as it penetrates radially through a fuel element, resulting in non-uniform reaction rate distributions [9]. This neutron flux attenuation is the result of self-shielding in the peripheral regions of the fuel, where U238 and other isotopes disproportionately absorb more flux than the center of the fuel. This effect

is distinctly pronounced in thermal reactors because neutrons born in the center of the fuel are less contributing to fission than neutrons arriving in towards the pellet, because neutrons have to thermalize in order to have an appreciable cross-section in thermal reactors [61]. This effect is especially pronounced in large fuel elements or those with high absorption cross-sections.

The impact of spatial self-shielding on the effective cross-section can be quantified with the disadvantage factor:

$$\xi = \frac{\phi_{avg}}{\phi_8} \quad (1.1)$$

where ϕ_{avg} is the average flux in the fuel element. This factor accounts for the flux depression within the fuel, which affects reaction rates and power distribution [10].

This disparity in flux and power results in harmful effects that reduce the lifespan of the fuel element, resulting most notably in the rim effect. The rim effect occurs when plutonium accumulation concentrates towards the rim of the pellet from increased U-238 capture, which leads to an increase in grain subdivision and porosity at the rim [11, 12]. This microstructural change will reduce the thermal conductivity in the rim region to additionally exacerbate the disparity in fuel temperature gradients.

In extreme cases, if burnup rates have been sustained above 75 GWd/tU, significant non-uniformity in flux can increase the probability of fuel fragmentation due to differential thermal expansion and stress accumulation [12]. Pellet fragmentation releases fission products and fuel particles into the helium gap between the fuel and cladding, increasing the probability of pellet-cladding mechanical interactions (PCMI) [13].

A simple solution to increase flux and reaction rate uniformity within a pellet is to tailor the enrichment and material compositions to relate to flux through its radius. To achieve a more uniform reaction rate across the fuel radius, we can vary the enrichment radially.

Several AM technologies enable the fabrication of such gradients in fuel geometries with heretofore unmatched precision, including binder jetting, digital light processing (DLP), fused deposition modeling (FDM), laser-oriented energy deposition, and powder bed fusion [3, 14, 13, 15].

These technologies provide considerable flexibility and customization for reactor core components. In addition to enhancing data collection and quality control via in-situ process monitoring, they ensure manufacturing efficiency and require fewer processes to produce heterogeneous fuels such as duplex and triplex fuels [8, 16].

1.2 Advanced Nuclear Fuel Fabrication

Additive manufacturing presents significant potential for reducing fabrication time and complexity while improving both neutronic and thermal-hydraulic performance. This manufacturing method is advantageous in terms of producing fuel pellets with uniform size and thickness and reducing deformation risks during fabrication. With AM, the risk of pulverization common in conventional manufacturing methods for monolithic fuels becomes minimal or non-existent [11]. Modern efforts have been invested into using parallelepiped solid fuel plates, ceramic and metallic microfluidics, or laser-powder bed fusion of Uranium niobium alloys to improve the performance of monolithic fuels [4]. Using AM to produce compositionally graded structures and heterogeneous duplex fuel architectures in monolithic forms could improve the economic performance of traditional fabrication techniques for the matrices of particle fuel forms [4, 17]. However, particle and dispersion fuels are further along in research for AM adoption due to the more straightforward process of qualifying Zr and Al matrices for AM than enriched uranium, which is inaccessible to most universities and laboratories [8]. However, particle and dispersion fuel architectures have a much lower power density [8] for most reactors that require extended periods without refueling.

For all fuel architectures, the ability of AM to manufacture fine-scale gradients and zones of enrichments, burnable absorbers, porosities, and dopants is of particular interest. Printers with multiple extruders or the ability to mix feedstocks in one extruder can be used, or individual materials may be printed and joined in post-processing [13].

There are six AM technologies that have been used to experimentally manufacture nuclear fuels; FDM, DLP, Stereolithography (SLA), binder jetting, laser-oriented energy deposition, and powder bed fusion. However, only FDM currently has the capability to manufacture ceramic UO_2 , as the UO_2 has a refractive index that is too high for lithography AM [8]. These characteristics hinder the curing process and make it challenging to achieve uniform, high-density sintering; however, thorium-compound fuels have been demonstrated to be produced with SLA and DLP due to having a higher refractive index [13].

FDM is the most ubiquitous and economical form of additive manufacturing, where an extruder melts a feedstock of material onto a bed in vertical layers to produce a desired part. Uranium Dioxide has been successfully manufactured with FDM at 100 μm resolution. However, this layer precision is limited by traditional internal gelation sol-gel methods, which produce ceramic fuel particles by chemically transforming a liquid solution into solid gel spheres. These methods, while suited for creating ceramic materials like UO_2 , struggle to generate particle diameters smaller than roughly 100 μm , which is significantly less precise compared to DLP and SLA methods, and poses challenges for FDM printing where finer

Table 1.1 AM Fuel architecture applications and characteristics [8, 11]

Fuel Architecture	Applications	Advantages	Disadvantages	Forms	Fabrication
Monolithic	All variants for commercial power, propulsion	Power Density, Heat transfer, Cost, Accepts minor actinide inclusion.	Steeper temperature gradients, retention of FPs during transients, mechanical integrity.	UO ₂ Pellets, U-Zr Casting, plates of UO ₂ clad in Al	Arc melting, then atomization and pulverisation into powder feedstock, and lastly cold pressing and sintering into cladding.
Dispersion	Research reactors, niche commercial reactors	Localizes fission-product damage. Metallurgically compatible with a wider array of fuel and matrix materials. Middle option between the simplicity and reduced cost of monolithic fuel, and the safety of particle fuels.	Power Density, Quality Control and Precision, Maximum Theoretical Packing Fraction limit is low due to intolerable swelling between adjacent dispersed fuel particles.	U-Al Matrix Plates	Chemical synthesis methods or mechanical milling produce crystallite U with sizes ranging from 0.01 to 0.1 mm. These are then distributed within a matrix using powder metallurgy techniques. Powder Cladding is cold rolled with this matrix into fuel plates, or consolidated with sintering and cold pressing..
Particle	Propulsion, Gas-Cooled reactors, Commercial reactors	Superior safety due to robust barriers against release of FPs; increased resistance to corrosion, oxidation, high temperatures, and neutron irradiation.	Power Density, Cost of Fabrication	Graphite or SiC TRISO, TRISO compacts, TRISO pellets.	Particle U kernels ranging from 0.3–1.0 mm or larger are dispersed in a Graphite or SiC matrix, then sintered with various layers to form fuel compact.

feedstock is required. Another challenge for FDM printing of ceramic fuels is the need for processing in inert atmospheres and concerns for criticality for enriched UO₂ [13].

However, in 2019, Moo et al. [13] addressed this concern by performing criticality simulations on FDM printing of highly enriched uranium and found no runaway criticality. Additionally, in 2023, Canada National Laboratory produced UO₂ printed fuel samples using FDM, successfully blending UO₂ with other compounds to produce compositional gradients and unique geometries [18, 19].

While AM techniques can withstand parameter variations during operation, the flexibility and suitability of a specific AM method to fabricate a compositional gradient is highly dependent on the AM technology [8]; lithography-oriented techniques can produce porosity gradients, but they cannot replicate gradual changes in a metal-alloy composition [8]. Inversely, FDM methods can produce compositional gradients using a wide range of materials,

Table 1.2 Benefits, challenges, and progress of additive manufacturing (AM) [8, 11, 13].

Fuel Architecture	A.M Potential Benefits	A.M Progress	A.M Challenges
Monolithic	Isotopic Gradients, Compositional Gradients, Engineered Porosity, geometry modifications, Reduced fabrication complexity for Metallic and duplex type fuels.	Laser-powder bed fusion of U-Nb alloys. Ceramic & Metallic Microfluidics adapted to internal gelation sol gel for synthesis of ceramic and metallic feedstocks below 50 μm diameter. Demonstration of fabricating a monolithic oxide pellet with a pseudo-duplex structure using surrogate materials, showing a compositional gradient. Stereolithographic production of high-density ThO ₂ .	Qualification and Licensure of new fuels. Regulation, economic, and material limitations reduce number of capable laboratories. Feedstock's particle size distribution and surface area. Difficulty in sourcing or preparation of acceptable feedstocks; UO ₂ 's absorbance values for STL, its oxidation at >300C in air, conventional sol gel feedstock production of diameters below 100 μm , and finally the need to debind and sinter in either inert or reducing environments. Viable UO ₂ surrogate.
Dispersion	Increased and novel Packing fractions, easier consolidation of discrete particles and dispersions into matrix, more extreme geometries, increased quality assurance, embedded sensing.	Medium	Lengthy time of irradiation testing and additional qualifications for matrices.
Particle	Increased and novel Packing fractions, easier consolidation of discrete particles and dispersions into matrix, more extreme geometries, increased quality assurance, embedded sensing	Binder Jet & chemical vapor infiltration used to produce SiC matrix without compaction & sintering, achieving .6 packing fraction, and novel geometries, enabling embedded sensing. Irradiation testing commenced. Tape casting fabrication; uniform packing fraction with controlled spacing for SiC matrix particle fuel forms.	Lengthy time of irradiation testing and additional qualifications for matrices.

though producing porosities is comparatively more challenging and crude, given the particle sizes of the feedstock and the attainable temperatures [13].

The use of ceramic materials for compositional grading has received limited attention compared to metal alloys, such as UZr, due to limited experience with freeze-form extrusion methods [20, 21]. However, alternating extruder nozzles containing different metal compounds (e.g., lithium iron phosphate and lithium titanate) have been demonstrated to work with ceramic feedstocks [8]. The challenges of materials with different chemical structures are absent if the desired final product and feedstock composition have homogeneous microstructure and chemistry; stark differences in the coefficient of thermal expansion will disturb the extrusion and adhesion of the fuel [8]. Loading UO₂ feedstock alongside a feedstock of a different compound, such as UB₂, into a single extruder for discretized variation is feasible, as is mixing the different compounds prior to solidification into a single feedstock [13]. Alternatively, FDM may simply use multiple extruders to vary the composition of nuclear fuels spatially within a component [12].

One of the main advantages of FDM is its ability to use multiple extruders simultaneously, or multiple feedstocks simultaneously, to produce finely-tuned enrichment gradients and burnable absorber gradients, enabling meticulous control over the distribution of fissile materials within each fuel pellet [8, 22]. As mentioned, the ability to tailor enrichment and burnable poison to a sub-millimeter scale has potential use for improving fuel utilization, as neutrons can be absorbed more efficiently throughout the pellet, maximizing burnup and reducing excess reactivity in low-flux regions [1]. This targeted approach enables improved fuel utilization, as neutrons can be absorbed more efficiently throughout the pellet, maximizing burnup and reducing excess reactivity in low-flux regions. Furthermore, various compounds and additives can be incorporated into the fuel matrix, including Neptunium to enhance anti-proliferation measures and Molybdenum to boost strength and thermal conductivity.

1.2.1 Fine-Scale Burnable Absorber Gradients

Burnable absorbers are equally important to the performance characteristics of a fuel assembly as the fuel itself. The rate of neutron absorption from the burnable absorber can offset excess reactivity, and the absorption rate of burnable absorbers, if matched with the burnup rate of fuel, can result in a relatively small reactivity swing if properly designed.

The degree to which burnable absorbers bend this reactivity swing, and when, can be very desirable if properly tailored to the fuel characteristics of its assembly. Fortunately, reactor designers have many options for choosing their burnable absorber. Gadolinium oxide has an absorption cross-section of 49,000 barns, while boron carbide has an absorption cross-section of only 759 barns [?]. Other options include erbium, yttrium, and hafnium, but the two options in wide production are the ultra-absorptive, quickly depleting gadolinium and the milder, slow-burning boron [5].

Gadolinium oxide (Gd_2O_3) is commonly added to light-water reactor (LWR) fuel to increase fuel loading within operational limits by reducing beginning-of-life (BoL) criticality. It is typically applied as a coating in thicknesses ranging from 2 to 4 microns, known as an Integral Fuel Burnable Absorber (IFBA). Gadolinium IFBA depletes rapidly within the first few months of reactor operation, reducing BoL criticality before allowing a rise in reactivity that reactor operators can anticipate and manage.

Gadolinium oxide may also be uniaxially pressed into a feedstock with uranium dioxide to create a homogeneous fuel-burnable absorber composition known as urania-gadolinia (UG), typically containing up to 10% (Gd_2O_3) by weight [5, 19]. Compared to IFBA, which involves a burnable absorber coating applied to the fuel pellet surface beneath the cladding, urania gadolinia mixed into the fuel depletes more gradually. This offers greater potential for

slowly reducing excess reactivity and decreasing the reliance on soluble boron for reactivity control [10].

A significant drawback of homogeneous urania-gadolinia fuels is gadolinia's relatively low coefficient of thermal conductivity. This property results in (Gd_2O_3) phases softening and expanding throughout the entirety of the pellet at peak operating conditions, which accelerates the hourglass effect, potentially reducing the overall lifetime of the fuel and possibly even leading to pellet-cladding mechanical interactions (PCMI) [13]. This has led to more discussions of discretizing (Gd_2O_3) phases towards the periphery of the pellet, where it can be utilized for BoL Keff more effectively [13], and towards the center of the pellet, where it can be used most effectively for gradual release [23].

The latter approach has led to the proposal of designs such as the Centrally-Shielded Burnable Absorber (CSBA). In CSBA proposals, a burnable absorber is placed as a sphere at the center of the fuel pellet, creating a shield that modifies the neutron flux distribution. This configuration reduces fast neutron flux in the central region, flattens the power distribution, and improves fuel utilization by reducing the risk of localized hot spots [23]. Similarly, the Centrally-Integrated Burnable Absorber (CIMBA) concept involves integrating a central rod of boron through the hole of annular fuel pellets, offering a more practical option for central fuel burnable absorber implementation [24].

While still promising for gradually curbing excess reactivity, introducing gadolinium or europium at levels exceeding just one thousand atomic parts per million can reduce thermal transport [5, 25, 26]. Introducing these reactivity control compounds into the fuel matrix can decrease the volume of fissile material within fuel rods and thus can negatively impact the overall cycle length of the core.

The use of IFBAs will be required to achieve longer fuel cycles that utilize high-assay low-enriched uranium (HALEU) fuel in LWRs [12, 19], but opportunities in Uranium Boride and other advanced nuclear fuels and absorbers may offset much of this limitation [27, 24]. Functionalized composite microstructures formed by adding a uranium boride phase to UO_2 are of interest for minimizing reactivity swing, especially in the context of additive manufacturing [8, 13, 12]. Incorporating uranium boride into a UO_2 matrix could offer the advantage of a more gradual burnable absorber, helping to mitigate the typical loss of fissile material associated with such absorbers. Additionally, these composite microstructures may enhance fuel performance by improving thermal conductivity or other beneficial properties

1.2.2 Fine-Scale Additives, Dopants, and Porosity Gradients

Compositional gradients could be leveraged in locating additives or dopants within metallic or ceramic fuels [8], which are mainly used to improve fuel performance [8, 28]. Additives

are added to metallic fuels to prevent cladding swelling and the migration of lanthanide fission products [29], while Dopants also have the capacity to improve thermal conductivity in uranium oxide [30, 8], however, mechanical effects are not uniform in all regions of the pellet.

1.3 Modeling

In this research, both deterministic lattice physics and stochastic Monte Carlo methods were employed for modeling and analyzing neutron behavior. These methods provide high-fidelity solutions by accounting for complex geometries, detailed energy spectra, and stochastic effects in neutron transport [31].

OpenMC, an open-source neutron transport code, uses continuous energy Monte Carlo methods and supports parallel execution via Message Passing Interface (MPI) and GPU acceleration. OpenMC is also capable of conducting k-eigenvalue calculations, and in this research, version 0.13.3 was used with the ENDF VIII.1 nuclear data library and integrated with the Distributed Evolutionary Algorithms in Python (DEAP) optimization framework [31].

Deterministic methods, such as the Winfrith Improved Multigroup Scheme (WIMS), offer a computationally efficient alternative by solving neutron transport equations using numerical techniques. However, during the early phases of this research, WIMS appeared inadequate for accurately capturing mutual shielding between resonant isotopes and self-shielding effects due to its reliance on older methods, such as the equivalence in dilution approach.

Recent work supports these findings, demonstrating that older versions of WIMS inaccurately predict radial reaction rate distributions. However, WIMS 11 and the DRAGON code have shown promising improvements in self-shielding accuracy, suggesting potential for future optimization workflows using deterministic methods [32].

OpenMC was selected for the optimization workflow due to its accurate handling of self-shielding and detailed geometries, which are critical for this research, and its flexible Python integration into diverse workflows to be able to adapt to various optimization requirements. Initial attempts with WIMS yielded poor results, and concerns about its self-shielding accuracy led to the decision to proceed with OpenMC. While WIMS 11 can perform resonance adjustments, OpenMC provided the necessary confidence for this study due to its integration with DEAP and its capacity for independent verification of results. OpenMC's role in this research strengthens its value as a reliable tool for future nuclear fine-scale fuel analysis and design work.

Chapter 2

Research Objectives

The emergence of novel fissile materials, burnable absorbers, and advanced manufacturing techniques demands a comprehensive re-evaluation of the boundaries of nuclear fuel design and performance.

There is much research at present for CSBA, CIMBA, and UB2 and Urania Gadolinia fuels, though research and modeling of AM fuels is very nascent. Recent studies by Moo et al. [13] have suggested a research need for gradients of burnable absorber in addition to gradients of enrichment.

Manufacturing UO_2 via FDM at sub-millimeter resolution is a demonstrated process [13]. Mixing feedstocks allows the incorporation of boron through Uranium diboride [33] or other burnable absorbers such as erbium and Gadolinium Oxide directly within the fissile material, eliminating reliance on external burnable absorbers. The relaxation of traditional manufacturing constraints, as well as computational advancement, has facilitated the exploration of more complex material distributions [34]. Because of this, the design for nuclear reactor fuels has expanded significantly. This growth has further required the development of optimization workflows designed for fine-scale fuel regions in order to exploit and improve this expanded design landscape efficiently [8].

Within this expanded design space, the most promising avenues for compositional gradients lie in the distribution of burnable absorber and fissile material. It stands to reason that increased enrichment heterogeneity within the fuel pins allows for a more synchronized relationship between neutron flux and corresponding enrichment levels, potentially improving fuel utilization. However, there will be a physical and economic limit to the degree to which these compositional gradients could improve performance [8, 13], and the CSBA concept remains theoretical and unproven compared to fuels with burnable absorber located towards their rim.

It is thus the intention of this paper to determine the optimal 100 μm -resolution spatial distribution of Uranium Dioxide, Uranium Diboride, and Gadolinium Oxide within the fuel meat of individual fuel pins to maximize attainable fuel utilization and operational lifetime, while minimizing reactivity swing and preserving adequate margin to safety limits.

To explore this design space, a multi-objective evolutionary algorithm is applied to a standard LWR fuel assembly to optimize enrichment and burnable absorber distributions, with the objective of maximizing end-of-life criticality (EoL K_{eff}) and minimizing reactivity swing and assembly power peaking factor (PPF).

The results from these optimization studies are compared with standard AP1000 fuel assemblies, including configurations with 2.35% and 4.45% enrichment, varying numbers of Pyrex rods, and differing quantities of IFBA. Finally, to assess whether performance improvements are due to the spatial distribution rather than the overall quantity of enrichment and burnable absorbers, the optimized assemblies are benchmarked against modified AP1000 fuel assemblies that contain the same total volumes of materials.

Chapter 3

Design Considerations

This research investigates the optimization of nuclear fuel design using a standard Westinghouse design LWR, the Westinghouse AP1000 design. Uranium Dioxide remains the primary fuel material due to its proven performance and extensive operational experience. The choice of Fused Deposition Modeling for manufacturing at 100-micron resolution represents a balance between achievable precision and practical manufacturability [13].

Recent advancements in iron-chromium-aluminum (FeCrAl) cladding materials have strongly mitigated hydrogen embrittlement fuel cladding degradation in LWRs [12]. Historically, hydrogen embrittlement degradation in cladding has been a significant limiting factor on the maximum fuel burnup achievable in an LWR. This potential advancement has sparked considerable interest within the research community regarding the feasibility and potential benefits of utilizing higher enrichments in the fuel for an AP1000 reactor [12].

Adopting these improved cladding materials enables easing burnup limitations; however, fully utilizing this additional headroom necessitates employing fuel with elevated fissile enrichment. High Assay Low Enriched Uranium (HALEU), which ranges between 5 and 19.75% enrichment, provides opportunities for extended fuel cycles and improved fuel utilization. However, it presents many challenges for use in LWRs [12].

In 2020, Oak Ridge National Lab (ORNL) performed neutronic and thermal analyses on an AP1000 with varying levels of High Assay Low Enriched (HALEU) enrichment [12]. In 2020, Brown et al. [12] discovered that as enrichment levels increased, there was a corresponding near-linear rise in phenomena, including resonance and spatial self-shielding and a more pronounced rim effect.

Notably, these effects featured even more pronounced segregation of burnup and plutonium accumulation towards the periphery of the fuel pellet. For HALEU, this drastic increase in disparity between the central and peripheral regions of the fuel pellet further warrants exploration into optimizing the compositions of those regions:

1. HALEU above 7% in existing LWRs exhibit intolerable levels of fission gas release, affecting fuel integrity and contributing to fuel pellet fragmentation at burnup levels in excess of 71 MWd/kgU;
2. the increase in the accumulation of plutonium towards the periphery complicates fuel behavior and increases logistical challenges for long-term waste management;
3. soluble boron coefficient decreases, necessitating more burnable absorbers, corrosive boric acid in the coolant and higher control rod worth;
4. the elevated fissile content also heightens the risk of accidental criticality during fuel handling and storage, necessitating more precise reactivity control [12].

This study uses Uranium Diboride (UB_2) and Gadolinium Oxide (Gd_2O_3) as burnable absorbers due to their contrasting. End-of-life criticality is the primary metric for evaluating fuel lifetime in the depletion studies performed with OpenMC. With this parameter, a reactor's capability to sustain criticality after a standard fuel cycle length of 18 months is measured. However, a second objective function was introduced post results to refine for more gradual burnup curves in favor over complete maximization of EOL KEFF. These simulations also prioritize the optimization of assembly PPF, ensuring that the highest PPF found at any depletion stage for the entire assembly is minimized without exceeding the threshold consistent with AP1000 operational limits.

Chapter 4

Methodology

4.1 Homogeneous Fuel Assembly Benchmarking

A standard, homogeneous AP1000 fuel assembly with an enrichment of 2.35% U-235 was modeled and simulated using OpenMC to:

1. **Establish Baseline Calibration:** Ensure that all geometries, materials, and simulation parameters accurately reflect industry standards for subsequent comparative studies.
2. **Provide a Benchmark for Optimization:** Serve as a reference point to evaluate the performance improvements achieved through optimization of fuel enrichment zoning and burnable absorber placement.

The fuel assembly was modeled as a quarter-symmetry section of a 17 AP1000 assembly with reflective boundary conditions. The model included guide tubes, zircalloy cladding, helium gaps, and water as the coolant. A regular mesh tally was implemented to calculate the fission rate distribution across the assembly.

The assembly was simulated at full power using OpenMC with the following parameters:

- **Batches:** 1,000 total batches (300 inactive)
- **Particles per Batch:** 50,000
- **Depletion Time Steps:** 0.5, 2, 3, 30, 90, 180, 270, 360, 450, 480, and 547.5 days

Table 4.1 Performance of Homogeneous AP1000 Fuel Assembly

Source	Enrichment	BOL keff	EOL keff	Max PPF
Design Control Document	2.35%	1.3364	0.99077	1.359
OpenMC Simulation	2.35%	1.3311	0.9901	1.357

Note: Soluble boron was deliberately excluded from all OpenMC simulations to simplify the simulation process and focus on the effects of fuel enrichment and burnable absorbers.

4.2 Integration of DEAP with OpenMC for Fuel Assembly Optimization

To explore the expanded design space enabled by additive manufacturing, particularly FDM, with a 100-micron maximum resolution, Python scripts were developed to integrate the Distributed Evolutionary Algorithms in Python (DEAP) framework with OpenMC simulations.

4.2.1 Optimization Case Studies Overview

Case Study A: Gadolinia Peripheral Optimization

- **Objective:** Optimize gadolinia (Gd_2O_3) content and enrichment levels in 12 intra-fuel pin zones (radial and axial) of the assembly. Gadolinia as IFBA at the periphery.
- **Variables:** Enrichment levels and gadolinia concentrations in fuel zones.
- **Generations:** 100
- **Depletion Chain:** Simplified Thermal with Gadolinium Isotopes

Case Study B: CSBA UB_2 Optimization

- **Objective:** Optimize uranium diboride (UB_2) content and enrichment levels in 4 zones, with UB_2 placed centrally in the fuel as a CSBA.
- **Variables:** Enrichment levels, UB_2 layer radius, and atom fraction of boron in the UB_2 zone.
- **Generations:** 20
- **Depletion Chain:** ENDF/B-VIII.0

4.2.2 Fuel Assembly Modeling

In all simulations performed, the fuel assemblies were a modified version of the benchmark assembly script; a quarter-symmetry section of a 17 AP1000 assembly with reflective boundaries, a mesh number of 9, complete with guide tubes, water as coolant, zircalloy cladding, and helium gaps, and benchmarked to be consistent with industry standards. Each fuel rod within the all assemblies were divided radially into four concentric fuel zones of equal volume, known as Fuel 1 through Fuel 4, representing the innermost to the outermost, respectively.

In study A, the 50 central fuel pins identified as the most problematic in power peaking consist of the same fuel zones but are surrounded by another layer. This additional layer is an optimized Gd_2O_3 IFBA layer. In study B, a UO_2 inner core of optimized radius is diluted with UB_2 at an optimized ratio, to serve as a longer-lasting burnable absorber. The thickness of each layer is optimized, for the IFBA between 1 and 9 microns as just a coating without any AM relation, and for UB_2 between 100 and 140 microns, with the atom fraction of Boron 10 and 11 in this mixture optimized between 0.1 and 1 atom fraction.

To maintain the total outer radius of the fuel rod (including the $\text{UO}_2\text{:UB}_2$ layer) constant, any change in the thickness of the $\text{UO}_2\text{:UB}_2$ layer necessitated corresponding adjustments to the fuel pellet radii, with a constraint on a minimum thickness of 100 microns for any region. The outer radius of the fourth fuel zone, $fr4$, is recalculated as:

$$fr4_{new} = R_{total} - t_{urbo} \quad (4.1)$$

Where $fr4_{new}$ is the variable radius of the outermost fuel zone, R_{total} is the fixed total outer radius of the fuel pin, and t_{urbo} is the thickness of the $\text{UO}_2\text{:UB}_2$ layer.

A scaling factor α was then determined:

$$\alpha = \frac{fr4_{new}}{FR4} \quad (4.2)$$

Here, $FR4$ represents the baseline outer radius of the fourth fuel zone. The inner fuel radii were scaled proportionally:

$$\begin{aligned} fr1 &= FR1 \times \alpha \\ fr2 &= fr1 + (FR2 - FR1) \times \alpha \\ fr3 &= fr2 + (FR3 - FR2) \times \alpha \end{aligned} \quad (4.3)$$

4.2.3 Script Parameters and Integration

Simulation Parameters:

- Initial Optimization Runs (First 12 generations):
 - Batches: 100 total batches (50 inactive)
 - Particles per Batch: 5,000
 - Depletion Time Steps: 109 days over five time steps (totaling 18 months)
 - * Integrator: CE/CM integrator selected for accuracy over fewer time steps
- Enhanced Optimization Runs (Study A):
 - Batches: 150 total batches (80 inactive)
 - Particles per Batch: 10,000
 - Depletion Time Steps: 54.75 days over ten time steps
- Final Verification Simulations:
 - Batches: 1,000 total batches (300 inactive)
 - Particles per Batch: 50,000
 - Depletion Time Steps: 0.5, 2, 3, 30, 90, 180, 270, 360, 450, 480, and 547.5 days

4.2.4 Objective Functions and Constraints:

The objective functions for each study were prioritized, in order, 1) EOL Keff, 2) BOL Keff, 3) PPF. The objective functions were as follows:

Objective Functions:

$$\begin{aligned}
 f_1(x) &= \text{BOL keff}(\text{maximize}) \\
 f_2(x) &= \text{EOL keff}(\text{maximize}) \\
 f_3(x) &= \text{PPF}(\text{minimize})
 \end{aligned}
 \tag{4.4}$$

Constraints:

$$\begin{aligned}
 1.15 &\leq \text{BOL keff} \leq 1.35 \\
 1.1 &\leq \text{EOL keff} \leq 1.35 \\
 1.0 &\leq \text{PPF} \leq 1.5
 \end{aligned}
 \tag{4.5}$$

The multi-objective optimization problem is addressed using a weighted sum approach, with the following composite fitness function:

$$F(x) = w_1 f_1(x) + w_2 f_2(x) - w_3 f_3(x) \quad (4.6)$$

Where:

$$\begin{aligned} w_1 &= 1.0(\text{weight for BOL keff maximization to constraint}) \\ w_2 &= 1.6(\text{weight for EOL keff maximization to constraint}) \\ w_3 &= 1.2(\text{weight for PPF minimization to constraint}) \end{aligned} \quad (4.7)$$

Table 4.2 Genetic Algorithm Parameters and Population Settings for Optimization Runs

Population Size	A:64, B:96,C:64
Generations	A:12,B:100,C:21
Variables	Continuous; A: 12, B: 13, C: 6
Mutation Probability	0.23
Mating Probability	0.47
Selection Operator	Selective Non-Dominated Sorting Genetic Algorithm II (selNSGA-II)
Mutation Operator	Polynomial
Mating Operator	Crossover Blend

However, after reviewing results, a second objective function was employed to better prioritize reactivity swing by removing EOL as an objective, and replacing it with minimization of difference between BOL and EOL KEFF, while BOL is being maximized and PPF minimized to the same constraints.

$$O = w_1 \times \frac{\text{BoL Keff}}{\text{BoL Keff}_{\max}} - w_2 \times \frac{\Delta \text{Keff}}{\Delta \text{Keff}_{\max}} - w_3 \times \frac{\text{PPF}}{\text{PPF}_{\max}} \quad (4.8)$$

Where:

$$\begin{aligned} w_1 &= 1.0(\text{weight for BOL keff maximization to constraint}) \\ w_2 &= 2(\text{weight for } \Delta \text{ Keff maximization to constraint}) \\ w_3 &= 1(\text{weight for PPF minimization to constraint}) \end{aligned} \quad (4.9)$$

4.3 Computational Workflow

Distributed Algorithms in Python (DEAP) is used to implement evolutionary algorithms for optimization, allowing for the generation, evaluation, and evolution of candidate fuel designs.

At initialization, a DEAP framework generates a population of potential fuel assembly designs (individuals) with varying parameters. The simulations are then run in parallel using multiprocessing across available CPU cores. PPF and Keff are calculated and recorded at each depletion stage. The parser script later calculates the overall performance, including maximum PPF and EoL Keff. OpenMC simulations are executed for each design. The parser script extracts criticality data for each depletion stage using the `openmc.StatePoint()` function. For PPF, the parser analyzes the fission rate distribution from mesh tallies, and the maximum local fission rate is normalized against the average to determine the PPF.

All studies employed the Selective Non-Dominated Sorting Genetic Algorithm II (seLNSGA-II) because of its more aggressive elitism and demonstrated use in the field of reactor optimization. seLNSGA-II selects individuals with elitism based on Pareto optimality, and then the blend crossover operator is used to produce offspring from these individuals by combining parent variables within a certain range defined; this method is advantageous for continuous variables. Polynomial mutation was chosen to avoid premature convergence.

4.4 Adjustments and Optimization Strategies

Initial coarser, lower-fidelity simulations were performed to identify potential Pareto fronts that could minimize the search space and reduce optimization convergence time. All simulations performed in OpenMC showed a higher fitness score for enrichment gradients concentrated towards the central region of the fuel pin, which allowed for the tightening of enrichment constraints after generation 30. In Study A (Gd_2O_3), after generation 50, a lack of individuals exhibiting maximum and minimum values in Uranium atom fraction and layer thickness variables prompted an increase in their constraints and their mutation probabilities, with a decrease in the crowding degree of the mutation, η , from 0.23 to 0.15.

Table 4.3 Optimization Constraints and Variable Limits for Fuel zones and UO₂/UB₂ layer

Variable	Minimum Constraint	Maximum Constraint
Fuel Zone 1, r1 (innermost)	3%	19.75%
Fuel Zone 2, r2	3%	19.75%
Fuel Zone 3, r3	2%	15%
Fuel Zone 4, r4 (outermost)	1%	10%
Cutback Fuel Zone 1, r5	3%	19.75%
Cutback Fuel Zone 2, r6	3%	19.75%
Cutback Fuel Zone 3, r7	2%	15%
Cutback Fuel Zone 4, r8	1%	10%
UO ₂ /UB ₂ Radius	100 microns	140 microns
Atom Fraction of U in UO ₂ /UB ₂ Layer	0.8	0.99

Table 4.4 Axial Zones and Layer Options for Fuel and Burnable Absorber Distribution

Fuel Zone	UO ₂ :UB ₂ or Gd ₂ O ₃ Layer Option	Corresponding Axial Zone
1,2,3,4	Yes	Main (Central Pin)
5,6,7,8	No	Upper Cutback
9,10,11,12	No	Lower Cutback

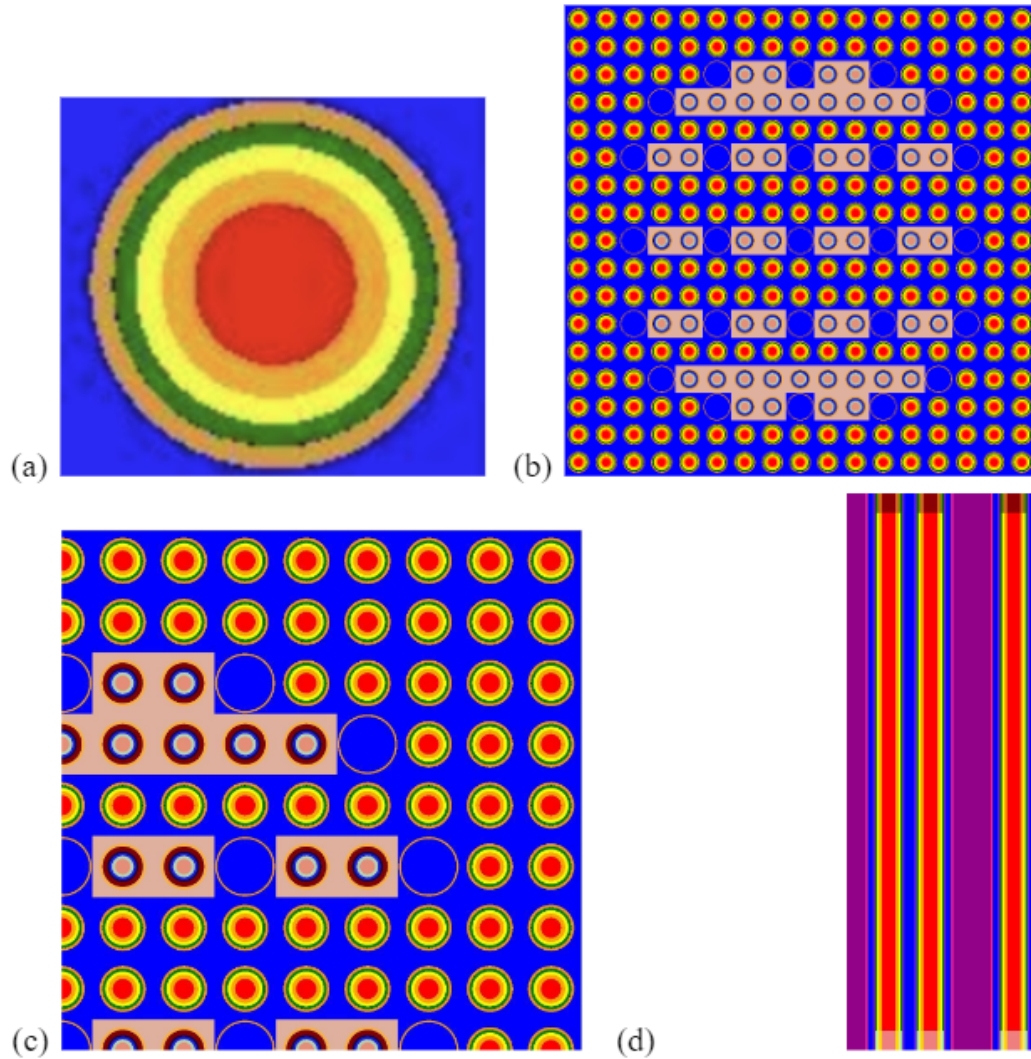


Fig. 4.1 The graphics above illustrate the zoned fuel assembly with homogenous enrichments, colored by material. Figure 1 A) illustrates one example of a fuel pin with four regions of enrichment, with this one being a CSBA design with the innermost red being zone 1 integrated with the UO:2UB2 at its maximum radius size; zone two is in orange, and the outermost green is zone four. The size of the outermost layer is at its maximum possible value. Figure 1(b) illustrates the $\frac{1}{4}$ symmetry of the assembly, while figure (1.c) shows the YZ-basis, which shows the upper and lower cutback regions. The fuel pins that are designated to contain gadolinium are highlighted by rectangles located towards the center of the core; in the UB2 study, all fuel pins are equal, and thus the UB2 dilution is high.

Chapter 5

Results

Note: All criticality plots (Keff vs Time, Keff vs PPF, Fuel Pin Normalized Power Distributions, Fuel Pin Normalized Fission Rate Distributions, Fuel Pin Normalized U238 Absorption Rate) are combined at the end of this section

5.1 Study A: Fine-Scale Multi-Objective Optimization of Enrichment and Gadolinia Zoning

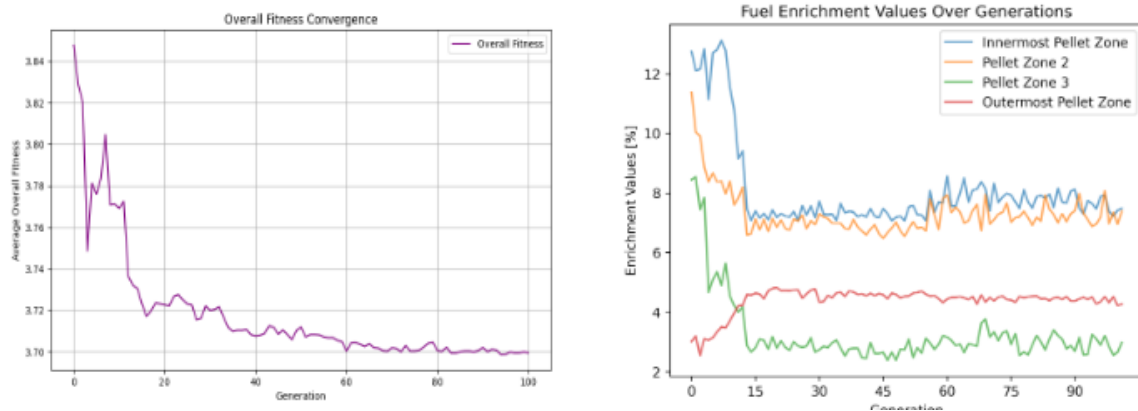


Fig. 5.1 Enrichment & Gadolinium Study Convergence Plot

5.1.1 Results A Discussion

The optimization reached 3.72 in fitness score after only 18 generations, though its best result came in generation 83, shown on the right. It is very important to note that this study was able to simulate 100 generations, 96 populations per generation because of the use of

Table 5.1 Optimized Fuel

Metric	Value
Beginning-of-Life (BOL) keff	1.3246
End-of-Life (EOL) keff	1.2002
Maximum Power Peaking Factor (PPF)	1.1465
Average Power Peaking Factor (PPF)	1.0931
Thickness of Gadolinium	.000124

Fuel Zone	Axial Region	Enrichment (%)
r1	Main (Central)	8.6574
r2	Main (Central)	2.0509
r3	Main (Central)	3.0091
r4	Main (Central)	2.5083
r5	Upper Cutback	5.4894
r6	Upper Cutback	6.5386
r7	Upper Cutback	7.1834
r8	Upper Cutback	4.9404
r9	Lower Cutback	9.0369
r10	Lower Cutback	17.2617
r11	Lower Cutback	2.4808
r12	Lower Cutback	4.2105

the simplified thermal depletion chain. Over 547.5 days, this is a significant uncertainty. However, verification of the optimized individual with ENDFB8 happened to result in very close results, which are the numbers presented, and still a slight improvement to the homogeneous reference.

On the other hand, the simplified depletion chain has a more pronounced effect on the individual with the highest overall fitness from the second objective function, the results presented (p.24). This second objective function determines a more gradual change in criticality but affords for lower overall EOL KEFF in comparison to the first objective function, and is plotted in the overall Keff charts.

Even though it was very quick per generation, it still took many days on 96 cores. It is clear from these results that the outermost layer, zone four, was increased in enrichment over time, while all other layers were minimized. The other layers fluctuated with slight progression in overall fitness for the next 80 generations, with a lot of undulation, which can be attributed to increased mutation and reduced crowding factors. These changes to the optimization were made in efforts to encourage greater exploration of the space, and to escape a local maxima.

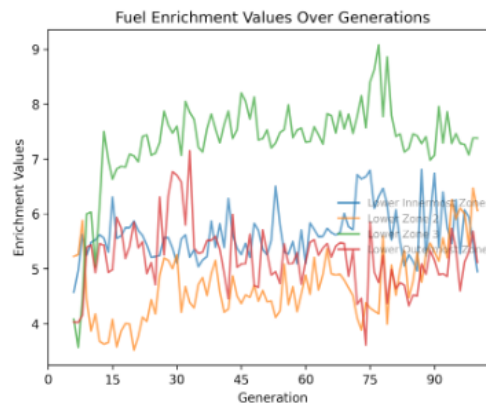


Fig. 5.2 Fuel Enrichment values Over Generations

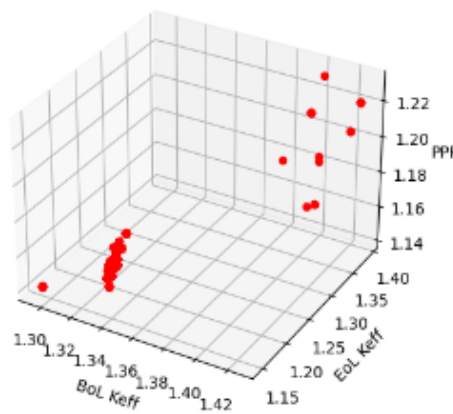


Fig. 5.3 3D Pareto Front for BOL Keff, EOL Keff. and PPF

The Pareto front shown is indicative of a local maxima, and the evolution of the gadolinium layer was nearly non-existent over the first 50 generations until stronger mutation was implemented. Yet, even still, the average main fuel region only received a modest increase in enrichment. While the average overall fitness continued to increase, it was clear that this layer was stubborn and even with reduced crowding factor; gadolinium was extremely absorptive, and the range provided was not large enough for its mutation to be very influential, despite gadolinia being incredibly potent.

Meanwhile, the cutback region fuels exhibited much stronger variation in enrichment than the other regions. The enrichment value of the third layer was dominating, with a much higher value than the rest, and clearly restricted the design space.

It is interesting that the main fuel region and cutback regions deviated so substantially in their progression, ranges, and overall values; in the standard AP1000 fuel assembly, the cutback region has less enrichment than the main region. The increase in zone 3 of the

cutback fuels suggest that it was favorable to combine higher enrichment with the proximity of the depleting absorber.

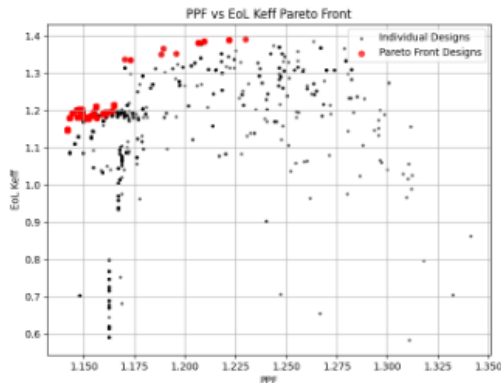


Fig. 5.4 Pareto Front for EOL KEFF vs PPF

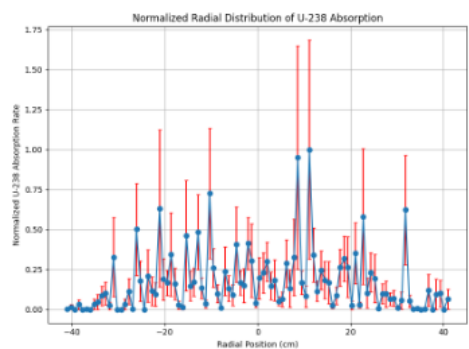


Fig. 5.5 U238 Absorption Rate Radial Profile

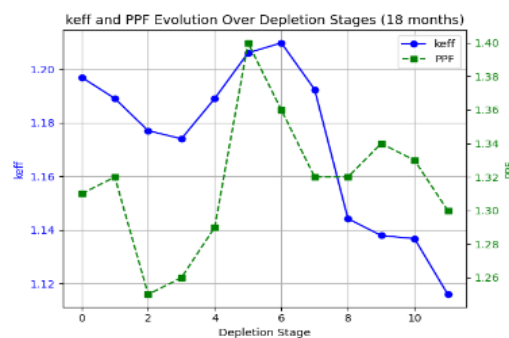


Fig. 5.6 Burnup vs PPF ove 18months for Design II

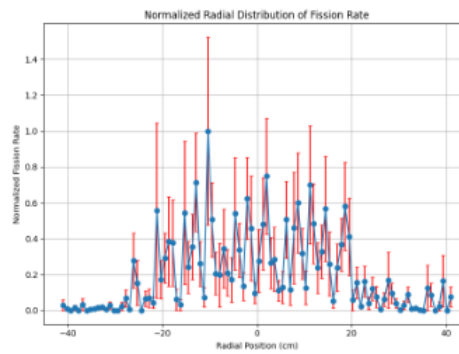


Fig. 5.7 Normalized Fission Rate Radial Distribution for Objective I

The burnup rate of the individual with the highest overall fitness is plotted against its homogeneous counterpart at the end on the next page. The overall amount of U-235 from four fuel zones of the optimized case was calculated and returned to be an equivalent of 7.13% over a one-zone fuel pin. The conclusions from their deviation in performance are harder to discern due to the presence of a burnable absorber in 50 inner fuel pins; however, the difference can still be examined once the gadolinium has depleted, and the radial flux and fission rate distributions are plotted.

The results for the second objective function produced a another well performing individual. Its performance is plotted on page 25.

Table 5.2 Optimized Reactor Performance Metrics

Metric	Value
Beginning-of-Life (BOL) keff	1.18
End-of-Life (EOL) keff	1.08
Maximum Power Peaking Factor (PPF)	1.23
Average Power Peaking Factor (PPF)	1.18


```

r1 = 7.324651690282735
r2 = 12.506420793191195
r3 = 2.923832724320935
r4 = 1.1840006743496128
r5 = 1.1840006743496128
r6 = 4.6519824410662265
r7 = 3.54677046905848
r8 = 7.503610033075448
r9 = 5.2399738275016965
r10 = 9.171802747184602
r11 = 4.480510475989577
r12 = 1.5219183632715647
t_ifba = 0.0005610568900411555

```

Fig. 5.8 Enrichments for 2nd Optimization Function

Note that the irregular shape for this criticality is a product of the chart more than the values themselves, and that it spikes very little in the center, but it does rise just slightly after much of the absorber has been burned off, but it still remains in the center. There is nearly five times as much Gadolinia in this individual when compared to the previous. The PPF for these studies are not comparable with the UB2 study, as the next study only consists of one fuel pin type whereas the Gadolinia study consists of two; one with and one without burnable absorbers. Notably, the homogeneous equivalent was 7.13%, which is the concentration at which ORNL previously recognized as a potential upper limit for HALEU in future LWRs [12].

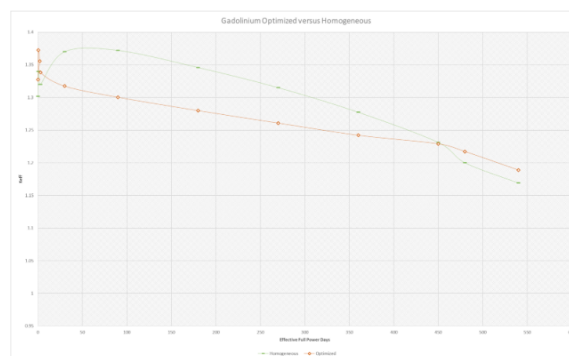


Fig. 5.9 Homogeneous 7.13% vs Optimized Fuel Assembly Design

5.2 CSBA Case Study

Discussion

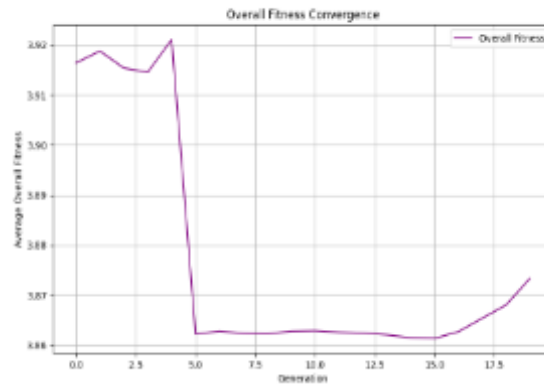


Fig. 5.10 Separated Optimization Convergence: Avg pop

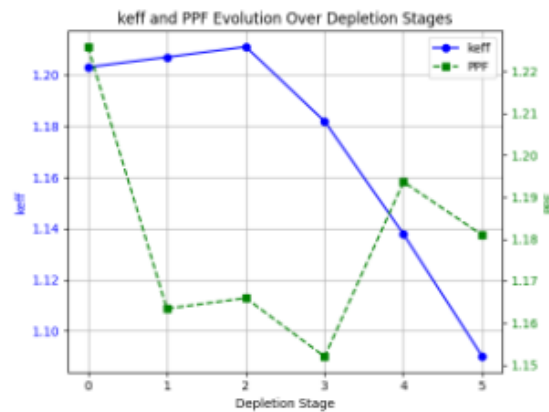


Fig. 5.11 Burnup vs PPF for best individual (18 months; 109 days per step, crude)

The optimization characteristics for study B were very similar to study A, except with far fewer generations, ENDF/B-VIII, a uniform fuel assembly, and a much lower overall enrichment due to UB2 being far less potent of an absorber. The optimization experienced a significant increase in fitness average early on when new constraints were applied to shrink the design space; enrichment ranges were lowered to 1-5%. The average population did not deviate much from the standard homogeneous case in the time allowed; however, the most fit individuals all had slight gradients toward the center. The PPF was the most limiting factor despite its more modest weight. The lack of significant deviation in enrichment between the zones is also in part owed to the tighter constraints allowing fewer options.

```

r1=4.01
r2=3.02
r3=2.87
r4=2.55
boron_mass_fraction_zone1= 0.0046

```

Fig. 5.12 Optimized Inputs for CSBA

Table 5.3 Optimized CSBA UB2 Design Metrics

Metric	Value
Beginning-of-Life (BOL) keff	1.197
End-of-Life (EOL) keff	1.08
Maximum Power Peaking Factor (PPF)	1.23
Average Power Peaking Factor (PPF)	1.18

There are not any pareto fronts provided given the lack of population and deviation in the sample.

The reason the enrichment rises in the center of the pellet, with zones one and two reliably ahead of three and four, is due to the optimizer choosing designs that best offset the concentration of burnable absorber, which increases in worth when there is increase in enrichment, and more neutrons fission at the center and less are absorbed by U238 in the rim due to reduced enrichment. The UB2 layer's boron atom fraction was slightly influential on PPF but clearly influential on Keff, and was rarely present near its minimum value in individuals of the populations. The objective function prioritized BOL and EOL Keff maximization, but with constraint on BOL at 1.35, which resulted in the UB2 layer being maximized more often than minimized, and the enrichments along with it. The radial distribution of all factors was much more flat than in the IFBA study, though both were performed for BOL, which discounts much of the effects that could be seen.

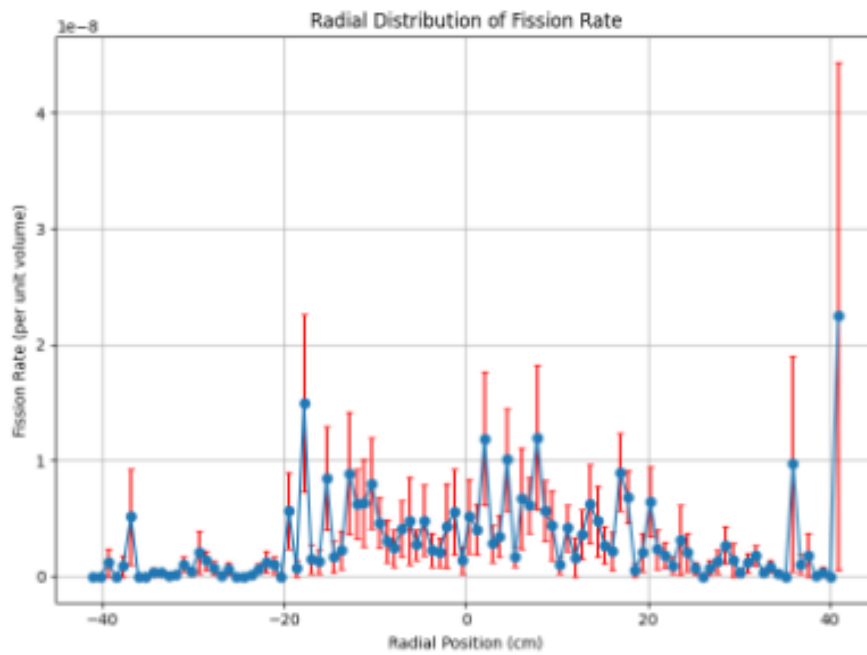


Fig. 5.13 CSBA: A Flatter Radial Distribution of Fission

Chapter 6

Conclusion

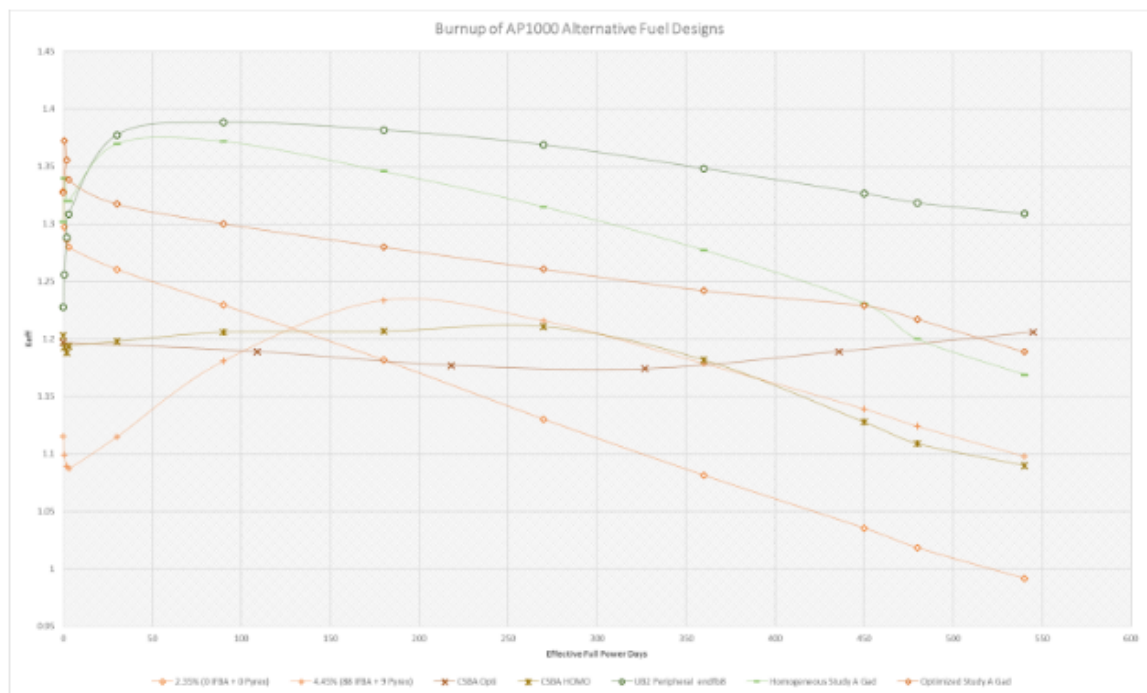


Fig. 6.1 CSBA Opti is Study B, CSBA Homo is its Homogeneous equivalent, UB2 Peripheral is the same boron overall volume, swapped into outer zone 4.

The optimization case studies revealed an intriguing trend in the enrichment distribution, with a pronounced shift of higher enrichment towards the core over generations. All simulations performed in OpenMC showed a higher fitness score for enrichment gradients concentrated towards the central region of the fuel pin; however, each had a BOL KEFF at least 5% less than their homogeneous counterparts, but only marginally better EOL KEFF. Notably, the outermost layer was rarely the smallest enrichment value, but the second inner layer was.

For both studies, the presence of burnable absorbers obscures the effect and thus should be examined on its own with more time and merit. There were simulations for no-absorber assemblies, and another for an assembly with another variable; location of the burnable absorber.

In order to fully optimize the fuel with AM capabilities, fully continuous variables in the radial and axial dimension for placement of burnable absorbers and enrichment gradients is a worthy successor to this work.¹ Furthermore, efforts were made to couple OpenMC with GPU offloading, which is nascent, but could be of great interest for optimization studies.

A longer term burnup study for space and naval propulsion using these advanced fuels would be of great significance. There are endless possibilities to improve fuel performance through optimization and A.M; perhaps even in the complexity of duplex and triplex fuels, where different isotopes of Thorium and Uranium could be optimized three dimensionally with the use of A.M technology.

With the ongoing development of new advanced fuels, rapidly evolving AM technology will remain highly relevant as a complementary tool in the exploitation of new fuel architectures and the incremental improvement of fuel performance through detailed combined codes. The ability to concentrate enrichment and burnable absorber towards the center of fuel is a feasible and worthy pursuit, whether they are for LWRs with more enrichment, or soluble-boron free small modular reactors.

¹<https://github.com/oliolio/diss>

References

- [1] I. Pioro and P. Kirillov, *Generation IV Nuclear Reactors as a Basis for Future Electricity Production in the World*, pp. 818–830. Formatex Research Center, 2013.
- [2] A. Aricò *et al.*, “Nanostructured materials for advanced energy conversion and storage devices,” *Nature Materials*, vol. 4, no. 5, pp. 366–377, 2005.
- [3] Y. Li *et al.*, “A review on functionally graded materials and structures via additive manufacturing: From multi-scale design to versatile functional properties,” *Advanced Materials Technologies*, vol. 5, no. 6, p. 1900981, 2020.
- [4] J. Simpson *et al.*, “Considerations for application of additive manufacturing to nuclear reactor core components,” tech. rep., Oak Ridge National Laboratory, Oak Ridge, TN, USA, 2019. Tech. Rep. ORNL/TM-2019/1190.
- [5] S. Mustafa and E. Amin, “The effect of soluble boron and gadolinium distribution on neutronic parameters of small modular reactor assembly,” *Radiation Physics and Chemistry*, vol. 171, p. 108724, 2020.
- [6] S. Alam, C. Goodwin, and G. Parks, “Assembly-level analyses of accident-tolerant cladding concepts for a long-life civil marine smr core using micro-heterogeneous duplex fuel,” *Progress in Nuclear Energy*, vol. 111, pp. 24–41, 2019.
- [7] T. Koyanagi, K. Terrani, S. Harrison, J. Liu, and Y. Katoh, “Additive manufacturing of silicon carbide for nuclear applications,” *Journal of Nuclear Materials*, vol. 543, p. 152577, 2021.
- [8] A. Nelson, “Prospects for additive manufacturing of nuclear fuel forms,” *Progress in Nuclear Energy*, vol. 155, p. 104493, 2023.
- [9] N. Badrun *et al.*, “Modeling of spert iv reactivity initiated transient tests in eureka-2/rr code,” *International Journal of Nuclear Energy*, 2014.
- [10] International Atomic Energy Agency (IAEA), “Neutron flux depression due to self-shielding in nuclear reactor fuel elements,” 2008. [Online]. Available: https://inis.iaea.org/collection/NCLCollectionStore/_Public/38/027/38027900.pdf.
- [11] N. Capps, R. Sweet, B. D. Wirth, A. Nelson, and K. Terrani, “Development and demonstration of a methodology to evaluate high burnup fuel susceptibility to pulverization under a loss of coolant transient,” *Nuclear Engineering and Design*, vol. 366, p. 110744, 2020.

- [12] J. R. Burns, R. Hernandez, K. A. Terrani, A. T. Nelson, and N. R. Brown, "Reactor and fuel cycle performance of light water reactor fuel with ^{235}U enrichments above 5%," *Annals of Nuclear Energy*, vol. 142, p. 107423, July 2020.
- [13] P. J. Moo, *Additive Manufacturing of Nuclear Materials by Digital Light Processing*. PhD thesis, University of Florida, 2021.
- [14] S. Zinkle, K. Terrani, and L. Snead, "Motivation for utilising new high-performance advanced materials in nuclear energy systems," *Current Opinion in Solid State and Materials Science*, vol. 20, no. 6, pp. 401–410, 2016.
- [15] O. O'Reilly-Hyland and G. T. Parks, "Additive manufacturing nuclear fuel design," tech. rep., University of Cambridge, September 2023.
- [16] C. Hensley *et al.*, "Qualification pathways for additively manufactured components for nuclear applications," *Journal of Nuclear Materials*, vol. 548, p. 152846, 2021.
- [17] E. Antolini, "Carbon supports for low-temperature fuel cell catalysts," *Applied Catalysis B: Environmental*, vol. 88, no. 1-2, pp. 1–24, 2009.
- [18] S. B. Alam *et al.*, "Small modular reactor core design for civil marine propulsion using micro-heterogeneous duplex fuel. part i: Assembly-level analysis," *Nuclear Engineering and Design*, vol. 346, pp. 157–175, May 2019.
- [19] M. Y. Mohsen, M. A. Abdel-Rahman, M. S. Hassan, and A. A. Galahom, "Searching for the most optimum burnable absorbers (bas) for ap-1000 from the neutronic, thermal-hydraulic, and solid mechanics points of view," *Nuclear Engineering and Design*, vol. 391, p. 111728, May 2022.
- [20] M. Leu *et al.*, "Freeze-form extrusion fabrication of functionally graded materials," *CIRP Annals*, vol. 61, no. 1, pp. 223–226, 2012.
- [21] J. Galloway *et al.*, "Modeling constituent redistribution in u–pu–zr metallic fuel using the advanced fuel performance code bison," *Nuclear Engineering and Design*, vol. 286, pp. 1–17, 2015.
- [22] R. Lucas, "3d printing a new nuclear future," *American Ceramic Society Bulletin*, vol. 101, pp. 48–51, September 2022.
- [23] Canada Makes, "Additive in industry: Exploring cnl's innovations in printing nuclear fuel," 2023. [Online]. Available: <https://canadamakes.ca/podcast/additive-in-industry-exploring-cnls-innovations-in-printing-nuclear-fuel-2023-09-27>.
- [24] X. H. Nguyen, C. H. Kim, and Y. Kim, "An advanced core design for a soluble-boron-free small modular reactor atom with centrally-shielded burnable absorber," *Nuclear Engineering and Technology*, 2018. [Online]. Available: <https://www.sciencedirect.com/science/article/pii/S1738573318305114>.
- [25] A. Arjunwadkar, P. Basu, and B. Acharya, "A review of some operation and maintenance issues of cfbc boilers," *Applied Thermal Engineering*, vol. 102, pp. 672–694, 2016.

- [26] Canadian Nuclear Laboratories, “A first for the nuclear industry: Cnl researchers successfully 3d print using uranium dioxide,” 2023. [Online]. Available: <https://www.cnl.ca/a-first-for-the-nuclear-industry-cnl-researchers-successfully-3d-print-using-uranium-dioxide/>.
- [27] B. Zohuri, *Generation IV Nuclear Reactors*, pp. 213–246. Woodhead Publishing, 2020.
- [28] Y. Che, G. Pastore, J. Hales, and K. Shirvan, “Modeling of Cr_2O_3 -doped UO_2 as a near-term accident tolerant fuel for lwrs using the bison code,” *Nuclear Engineering and Design*, vol. 337, pp. 271–278, 2018.
- [29] C. Sun *et al.*, “Additive manufacturing for energy: A review,” *Applied Energy*, vol. 282, p. 116041, 2021.
- [30] S. Pokrovskiy, V. Baranov, and A. Tenishev, “Thermal properties of $(\text{Al}, \text{Gd})\text{O}_3$ doped uranium dioxide,” *IOP Conference Series: Materials Science and Engineering*, vol. 130, p. 012026, 2016.
- [31] K. Wang *et al.*, “Rmc—a monte carlo code for reactor core analysis,” *Annals of Nuclear Energy*, vol. 82, pp. 121–129, 2015.
- [32] R. Refeat and B. Foad, “Assessment of resonance self-shielding models during burn-up calculations,” *Journal of Materials Science and Engineering A*, vol. 11, no. 7–9, pp. 96–105, 2021.
- [33] A. Ramadhan, A. Suwono, E. Umar, and N. Tandian, “Preliminary study for design core of nuclear research reactor of triga bandung using fuel element plate mtr,” *Engineering Journal*, vol. 21, no. 3, pp. 173–181, 2017.
- [34] K. Eckelmeyer, “Uranium and uranium alloys,” 1990.
- [35] Z. Mian, M. Ramana, and A. Nayyar, “Nuclear submarines in south asia: New risks and dangers,” *Journal for Peace and Nuclear Disarmament*, vol. 2, no. 1, pp. 184–202, 2019.
- [36] H. Chiswik *et al.*, “Advances in the physical metallurgy of uranium and its alloys,” tech. rep., Argonne National Laboratory, Lemont, IL, USA, 1958.
- [37] H. Peacock and R. Frontroth, “Properties of aluminum-uranium alloys,” tech. rep., Savannah River Site (SRS), Aiken, SC, USA, 1989.
- [38] T. Allen, J. Busby, R. Klueh, S. Maloy, and M. Toloczko, “Cladding and duct materials for advanced nuclear recycle reactors,” *JOM*, vol. 60, no. 1, pp. 15–23, 2008.
- [39] K. Rao *et al.*, “Dynamic fault tree analysis using monte carlo simulation in probabilistic safety assessment,” *Reliability Engineering & System Safety*, vol. 94, no. 4, pp. 872–883, 2009.
- [40] J. Crocker and L. Stephan, “Reactor power excursion tests in the spert iv facility,” Tech. Rep. IDO-17000, Phillips Petroleum Co., Atomic Energy Division, Idaho Falls, ID, USA, 1964.

- [41] L. Foulds, *Optimization Techniques: An Introduction*. Springer Science & Business Media, 2012.
- [42] M. Bhatti, *Practical Optimization Methods: With Mathematica® Applications*. Springer Science & Business Media, 2012.
- [43] L. Collatz and W. Wetterling, *Optimization Problems*, vol. 17. Springer Science & Business Media, 2012.
- [44] U. Diwekar, *Introduction to Applied Optimization*, vol. 22. Springer Nature, 2020.
- [45] A. Zomaya, C. Ward, and B. Macey, “Genetic scheduling for parallel processor systems: Comparative studies and performance issues,” *IEEE Transactions on Parallel and Distributed Systems*, vol. 10, no. 8, pp. 795–812, 1999.
- [46] K. Matouš, M. Lepš, J. Zeman, and M. Šejnoha, “Applying genetic algorithms to selected topics commonly encountered in engineering practice,” *Computer Methods in Applied Mechanics and Engineering*, vol. 190, no. 13–14, pp. 1629–1650, 2000.
- [47] Y. Choi and H. Stenger, “Water gas shift reaction kinetics and reactor modeling for fuel cell grade hydrogen,” *Journal of Power Sources*, vol. 124, no. 2, pp. 432–439, 2003.
- [48] S. Choy, C. Sun, K. Leong, and J. Wei, “Compressive properties of functionally graded lattice structures manufactured by selective laser melting,” *Materials & Design*, vol. 131, pp. 112–120, 2017.
- [49] F. Glover, J. Kelly, and M. Laguna, “Genetic algorithms and tabu search: Hybrids for optimization,” *Computers & Operations Research*, vol. 22, no. 1, pp. 111–134, 1995.
- [50] G. Gündüz, T. Uslu, and H. Durmazuçar, “Boron-nitride-coated nuclear fuels,” *Nuclear Technology*, vol. 116, no. 1, pp. 78–90, 1996.
- [51] J. Hirschhorn *et al.*, “Metallic fuel performance benchmarks for versatile test reactor applications,” *Nuclear Science and Engineering*, vol. 196, no. sup1, pp. 123–147, 2022.
- [52] A. Hoang, T. Nguyen, and B. Nguyen, “The novel design of feed-water control system for thermal power plant using super-critical start-up motor-boiler feed-water pump,” in *Proc. 2020 IEEE PES/IAS PowerAfrica*, pp. 1–5, 2020.
- [53] I. Kratochvílová *et al.*, “Nanosized polycrystalline diamond cladding for surface protection of zirconium nuclear fuel tubes,” *Journal of Materials Processing Technology*, vol. 214, no. 11, pp. 2600–2605, 2014.
- [54] M. Meyer *et al.*, “Irradiation performance of u-mo monolithic fuel,” *Nuclear Engineering and Technology*, vol. 46, no. 2, pp. 169–182, 2014.
- [55] S. S. Rao, *Engineering Optimization: Theory and Practice*. John Wiley & Sons, 5th ed., 2019.
- [56] J. Škarohlíd *et al.*, “Nanocrystalline diamond protects zr cladding surface against oxygen and hydrogen uptake: Nuclear fuel durability enhancement,” *Scientific Reports*, vol. 7, no. 1, p. 6469, 2017.

- [57] H. Yu, D. Hartanto, J. Moon, and Y. Kim, “A conceptual study of a supercritical CO₂-cooled micro modular reactor,” *Energies*, vol. 8, no. 12, pp. 13938–13952, 2015.
- [58] T. Zhang *et al.*, “Conceptual design of an innovative reduced moderation thorium-fueled small modular reactor with heavy-water coolant,” *International Journal of Energy Research*, vol. 43, no. 14, pp. 8286–8298, 2019.
- [59] G. J. Y. Chee, *Fluoride-Salt-Cooled High-Temperature Reactor Generative Design Optimization with Evolutionary Algorithms*. PhD thesis, University of Illinois at Urbana-Champaign, 2022.
- [60] E. Sprague, “Characterization of direct metal deposition printed copper-iron alloys,” Master’s thesis, University (unspecified). [Unpublished Master’s thesis].
- [61] W. Lee *et al.*, “Innovative-smr design with cimba fuel using two-step code stream2d/rastk.” [Conference or Journal], [Year]. [Incomplete reference, publication details needed].
- [62] J. R. Lamarsh and A. J. Baratta, *Introduction to Nuclear Engineering*. Pearson, 4th ed., 2017.

Appendix A

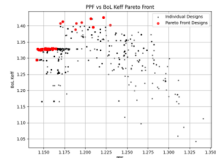


Fig. A.1 PPF vs BoL Keff Pareto Front, Study A

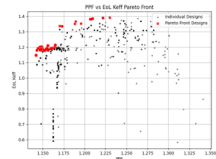


Fig. A.2 Final generation pareto front Case Study A

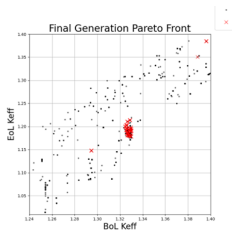


Fig. A.3 3D pareto front for BoL Keff, EoL Keff, and PPF

3D Pareto Front for BOL Keff, EOL Keff, and PPF

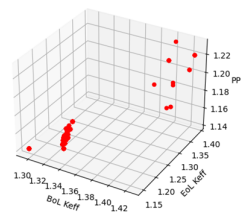


Fig. A.4 UB2 No Bo Depletion Study

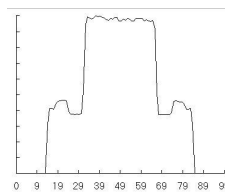


Fig. A.5 Hypervolume progression over generations

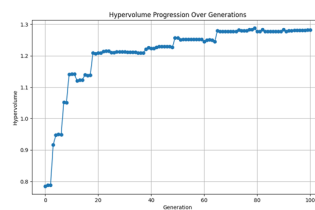


Fig. A.6 PPF vs EoL Keff pareto front

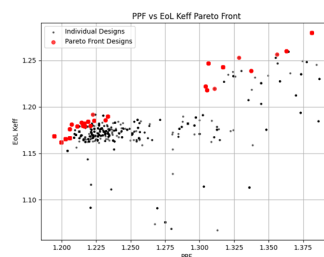


Fig. A.7 UB2 layer radius v. atom fraction in UB2 (failed study; UB2 not depletable in this one, hence 100 generations)

Study B CSBA Optimization:

```
import os
import openmc
import numpy as np
import openmc.deplete
# csba
ROOT_DIR = "/home/hpcatta/openmc-0.13.3/please/runcsba/"
DEPLETION_FILE = "/home/hpcatta/openmc-0.13.3/please/chain_endfb80_pwr."
CROSS_SECTION_FILE = '/home/hpcatta/openmc/endfb-viii.0-hdf5/cross_section'

ENRICHMENT_VALUES = "enrichments.txt"
RADIUS_VALUES = "fuel_radius.txt"

time_step_nr = 5

def get_cross_sections():
    os.environ['OPENMC_CROSS_SECTIONS'] = os.path.abspath(CROSS_SECTION_FILE)
    openmc.config['cross_sections'] = CROSS_SECTION_FILE

get_cross_sections()

# r1 = {{r1}}
# r2 = {{r2}}
# r3 = {{r3}}
# r4 = {{r4}}
# boron_mass_fraction_zone1 = 0.001
# fr1 = {{fr1}}
```

```
# Optimizable parameters
```

```
boron_mass_fraction_zone1 = 0.007979793401428615
```

```
fr1 = 0.11050140207233414 # Radius of zone 1
```

```
FUEL_OUTER_RADIUS = 0.415 # Fixed outer radius
```

```
FR1_REF = 0.20475 # Reference radius for zone 1
```

```
FR2_REF = 0.28956
```

```
FR3_REF = 0.35464
```

```
FR4_REF = 0.4095
```

```
def save_radius_values(fr1 , fr2 , fr3 , fr4 ):
```

```
    try :
```

```
        gen_pop = os.path.split(os.path.abspath(os.curdir))[-1].split(" ")
```

```
        gen = gen_pop[0]
```

```
        pop = gen_pop[1]
```

```
    except IndexError:
```

```
        gen = "unknown"
```

```
        pop = "unknown"
```

```
    with open(os.path.join(ROOT_DIR, RADIUS_VALUES), 'a') as file:
```

```
        line = f"{gen} {pop} {fr1} {fr2} {fr3} {fr4} {FUEL_OUTER_RADIUS}"
```

```
        file.write(line)
```

```
def get_fuel_radius_values():  
    alpha = fr1 / FR1_REF # Scaling factor based on fr1  
    fr2 = fr1 + (FR2_REF - FR1_REF) * alpha  
    fr3 = fr2 + (FR3_REF - FR2_REF) * alpha  
    fr4 = FUEL_OUTER_RADIUS # Fixed outer radius  
    return fr1, fr2, fr3, fr4  
  
def run_calculation(r1_, r2_, r3_, r4_):  
    plot_pixels = 1200  
    mesh_nr = 9  
  
def define_universe_components(r1_, r2_, r3_, r4_, no_of_pins):  
    fr1, fr2, fr3, fr4 = get_fuel_radius_values()  
    save_radius_values(fr1, fr2, fr3, fr4)  
    fuel_radius1 = openmc.ZCylinder(r=fr1)  
    fuel_radius2 = openmc.ZCylinder(r=fr2)  
    fuel_radius3 = openmc.ZCylinder(r=fr3)  
    fuel_outer_radius = openmc.ZCylinder(r=fr4)  
    clad_inner_radius = openmc.ZCylinder(r=0.4177)  
    clad_outer_radius = openmc.ZCylinder(r=0.4749)  
    gt_inner_radius = openmc.ZCylinder(r=0.5715)  
    gt_outer_radius = openmc.ZCylinder(r=0.612)  
    lower_cutback_height = openmc.ZPlane(z0=-426.0 / 2.0 + 15)  
    upper_cutback_height = openmc.ZPlane(z0=+426.0 / 2.0 - 15)  
    fuel_bottom = openmc.ZPlane(z0=-426.0 / 2.0, boundary_type='ref
```



```
fuel_top = openmc.ZPlane(z0=+426.0 / 2.0, boundary_type='reflective')

materials = openmc.Materials([])

# Adjusting mass fractions to include boron in Fuel 1
total_mass_fraction = 1.0
remaining_mass_fraction = total_mass_fraction - boron_mass_fraction
uranium_mass_fraction = 0.8815 * remaining_mass_fraction
oxygen_mass_fraction = 0.1185 * remaining_mass_fraction

f_1 = openmc.Material(name='Fuel 1')
f_1.add_element('U', uranium_mass_fraction, enrichment=r1_, percent_type='w')
f_1.add_nuclide('O16', oxygen_mass_fraction, percent_type='w')
f_1.add_nuclide('B10', boron_mass_fraction_zone1 * 0.16, percent_type='w')
f_1.add_nuclide('B11', boron_mass_fraction_zone1 * 0.84, percent_type='w')
f_1.set_density('g/cc', 10.4)
f_1.volume = (np.pi * fuel_radius1.r ** 2) * 396 * no_of_pins
materials += [f_1]

f_2 = openmc.Material(name='Fuel 2')
f_2.add_element('U', 1.0, enrichment=r2_)
f_2.add_nuclide('O16', 2.0)
f_2.set_density('g/cc', 10.4)
f_2.volume = np.pi * (fuel_radius2.r ** 2 - fuel_radius1.r ** 2) * 396 * no_of_pins
materials += [f_2]
```

```
f_3 = openmc.Material(name='Fuel 3')
f_3.add_element('U', 1.0, enrichment=r3_)
f_3.add_nuclide('O16', 2.0)
f_3.set_density('g/cc', 10.4)
f_3.volume = np.pi * (fuel_radius3.r ** 2 - fuel_radius2.r ** 2)
materials += [f_3]

f_4 = openmc.Material(name='Fuel 4')
f_4.add_element('U', 1.0, enrichment=r4_)
f_4.add_nuclide('O16', 2.0)
f_4.set_density('g/cc', 10.4)
f_4.volume = np.pi * (fuel_outer_radius.r ** 2 - fuel_radius3.r ** 2)
materials += [f_4]

r_cutback = r1_ - 0.5

f_cutback = openmc.Material(name='Fuel Cutback')
f_cutback.add_element('U', 1.0, enrichment=r_cutback)
f_cutback.add_nuclide('O16', 2.0)
f_cutback.set_density('g/cc', 10.4)
f_cutback.volume = (np.pi * fuel_outer_radius.r ** 2) * 30 * no
materials += [f_cutback]

zircaloy = openmc.Material(name='Zircaloy -4')
zircaloy.add_element('Zr', 0.9811, percent_type='wo')
zircaloy.add_element('Sn', 0.0067, percent_type='wo')
```

```
zircaloy.add_element('Nb', 0.01, percent_type='wo')
zircaloy.add_element('O', 0.0012, percent_type='wo')
zircaloy.set_density('g/cm3', 6.55)
```

```
helium = openmc.Material(name='Helium')
helium.add_element('He', 1.0)
helium.set_density('g/cm3', 0.178e-3)
```

```
water = openmc.Material(name='water')
water.add_nuclide('H1', 2.0)
water.add_nuclide('O16', 1.0)
water.set_density('g/cm3', 1.0)
water.add_s_alpha_beta('c_H_in_H2O')
```

```
materials += [helium, zirconium, water]
```

```
materials.export_to_xml()
```

```
fuel1_region = -fuel_radius1 & +lower_cutback_height & -upper_c
fuel2_region = +fuel_radius1 & -fuel_radius2 & +lower_cutback_h
fuel3_region = +fuel_radius2 & -fuel_radius3 & +lower_cutback_h
fuel4_region = +fuel_radius3 & -fuel_outer_radius & +lower_cutb
```

```
cutback_region = (-fuel_outer_radius & -lower_cutback_height &
```

```
gap_region = +fuel_outer_radius & -clad_inner_radius & +fuel_bo
```

```
clad_region = +clad_inner_radius & -clad_outer_radius & +fuel_b
```

```
gt_water_region = -gt_inner_radius & +fuel_bottom & -fuel_top
```

```
gt_clad_region = +gt_inner_radius & -gt_outer_radius & +fuel_bo
```

```
fuel1 = openmc.Cell(name='fuel1 ')
```

```
fuel1.fill = f_1
```

```
fuel1.region = fuel1_region
```

```
fuel2 = openmc.Cell(name='fuel2 ')
```

```
fuel2.fill = f_2
```

```
fuel2.region = fuel2_region
```

```
fuel3 = openmc.Cell(name='fuel3 ')
```

```
fuel3.fill = f_3
```

```
fuel3.region = fuel3_region
```

```
fuel4 = openmc.Cell(name='fuel4 ')
```

```
fuel4.fill = f_4
```

```
fuel4.region = fuel4_region
```

```
cutback = openmc.Cell(name='Cutback ')
```

```
cutback.fill = f_cutback
```

```
cutback.region = cutback_region
```

```
gap = openmc.Cell(name='air gap ')
```

```

gap.region = gap_region
gap.fill = helium

clad = openmc.Cell(name='clad ')
clad.fill = zirconium
clad.region = clad_region

moderator = openmc.Cell(name='Moderator ', fill=water ,
                        region=+clad_outer_radius & -fuel_top &

return (gt_outer_radius , fuel_bottom , fuel_top , f_1 , f_2 , f_3 ,
        zirconium , water , gt_water_region , gt_clad_region , fuel
        gap , clad , moderator)

(gt_outer_radius , fuel_bottom , fuel_top , f_1 , f_2 , f_3 , f_4 , f_cutb
zirconium , water , gt_water_region , gt_clad_region , fuel1 , fuel2 , f
gap , clad , moderator) = define_universe_components(r1__ , r2__ , r3__

gt1 = openmc.Cell(name='Guide tube filled with water ', fill=water ,
gt2 = openmc.Cell(name='Guide tube clad ', fill=zirconium , region=gt
mode = openmc.Cell(name='Moderator ', fill=water ,
                    region=+gt_outer_radius & -fuel_top & +fuel_botto
gt = openmc.Universe(name='Guide Tube ', cells=[gt1 , gt2 , mode])

pin_cell_universe = openmc.Universe(name='Fuel Pin ', cells=[
    fuel1 , fuel2 , fuel3 , fuel4 , cutback , gap , clad , moderator])

```

```
pitch = 1.26
```

```
assembly = openmc.RectLattice(name='Fuel - OBA')
```

```
assembly.pitch = (pitch, pitch)
```

```
assembly.lower_left = [-pitch * mesh_nr / 2] * 2
```

```
assembly.universes = [
```

```
    [pin_cell_universe for _ in range(mesh_nr)],
```

```
    [pin_cell_universe for _ in range(mesh_nr)],
```

```
    [pin_cell_universe for _ in range(5)] + [gt] + [pin_cell_univer
```

```
    [pin_cell_universe for _ in range(3)] + [gt] + [pin_cell_univer
```

```
    [pin_cell_universe for _ in range(mesh_nr)],
```

```
    [pin_cell_universe for _ in range(2)] + [gt] + [pin_cell_univer
```

```
    [pin_cell_universe for _ in range(mesh_nr)],
```

```
    [pin_cell_universe for _ in range(mesh_nr)],
```

```
    [pin_cell_universe for _ in range(2)] + [gt] + [pin_cell_univer
```

```
]

```

```
root_cell = openmc.Cell(name='root cell', fill=assembly)
```

```
min_x = openmc.XPlane(x0=-pitch * mesh_nr / 2, boundary_type='refle
```

```
max_x = openmc.XPlane(x0=pitch * mesh_nr / 2, boundary_type='reflec
```

```
min_y = openmc.YPlane(y0=-pitch * mesh_nr / 2, boundary_type='refle
```

```
max_y = openmc.YPlane(y0=pitch * mesh_nr / 2, boundary_type='reflec
```

```
root_cell.region = +min_x & -max_x & +min_y & -max_y & +fuel_bottom
```

```
root_universe = openmc.Universe(name='root universe')
root_universe.add_cell(root_cell)
```

```
geometry = openmc.Geometry(root_universe)
geometry.export_to_xml()
```

```
point = openmc.stats.Point((0, 0, 0))
source = openmc.source.Source(space=point)
```

```
settings = openmc.Settings()
settings.source = source
settings.batches = 150
settings.inactive = 80
settings.particles = 10000
settings.export_to_xml()
```

```
tallies = openmc.Tallies()
mesh = openmc.RegularMesh(mesh_id=1)
mesh.dimension = [mesh_nr, mesh_nr]
mesh.lower_left = [-pitch * mesh_nr / 2] * 2
mesh.width = [pitch, pitch]
```

```
mesh_filter = openmc.MeshFilter(mesh)
```

```
tally = openmc.Tally(name='mesh tally')
```

```
tally.filters = [mesh_filter]
```

```
tally.scores = ['fission']
```

```
tallies.append(tally)
```

```
tallies.export_to_xml()
```

```
plot1 = openmc.Plot()
```

```
plot1.filename = 'pinplot'
```

```
plot1.origin = (0, 0, 0)
```

```
plot1.width = (pitch * mesh_nr, pitch * mesh_nr)
```

```
plot1.pixels = (plot_pixels, plot_pixels)
```

```
plot1.color_by = 'material'
```

```
plot1.colors = {f_1: 'red', f_2: 'orange', f_3: 'yellow', f_4: 'green',  
                f_cutback: 'gray'}
```

```
plot2 = openmc.Plot()
```

```
plot2.filename = 'XY basis'
```

```
plot2.basis = 'xy'
```

```
plot2.origin = (0, 0, 0)
```

```
plot2.width = (pitch * mesh_nr, pitch * mesh_nr)
```

```
plot2.pixels = (plot_pixels, plot_pixels)
```

```
plot2.color_by = 'material'
```

```
plot2.colors = {f_1: 'red', f_2: 'orange', f_3: 'yellow', f_4: 'green',  
                f_cutback: 'gray'}
```

```
plot3 = openmc.Plot()
```



```
plot3.filename = 'YZ basis'
plot3.basis = 'yz'
plot3.width = (pitch * mesh_nr, 426)
plot3.pixels = (plot_pixels, plot_pixels)
plot3.color_by = 'cell'
plot3.colors = {f_1: 'red', f_2: 'orange', f_3: 'yellow', f_4: 'green',
                f_cutback: 'gray'}
```



```
plots = openmc.Plots([plot1, plot2, plot3])
plots.export_to_xml()
```



```
model = openmc.Model(geometry=geometry, settings=settings)
model.export_to_xml()
operator = openmc.deplete.CoupledOperator(model, DEPLETION_FILE)
power = 21.75E06 / 4
time_steps = [109.5] * time_step_nr
integrator = openmc.deplete.CECMIntegrator(operator, time_steps, power)
integrator.integrate()
```



```
import os
import openmc
import numpy as np
import openmc.deplete
```



```
# Update save_enrichments to track boron_mass_fraction_zone1
def save_enrichments():
    """Enrichments shall be saved into file along with boron_mass_fraction_zone1"""
```

```
try:
    gen_pop = os.path.split(os.path.abspath(os.curdir))[-1].split("/")
    gen = gen_pop[0]
    pop = gen_pop[1]
except IndexError:
    gen = "unknown"
    pop = "unknown"

with open(os.path.join(ROOT_DIR, ENRICHMENT_VALUES), 'a') as file:
    line = f"{gen} {pop} {r1} {r2} {r3} {r4} {boron_mass_fraction_z}"
    file.write(line)

# Call these updated functions where necessary, passing boron_mass_frac

save_enrichments()
run_calculation(r1, r2, r3, r4)
```